Volume 11 | Issue 1 Article 8

2022

Stratospheric Effects on UV, Speed of Sound, Pressure, and Temperature

Joshua V. Chis
DePaul University, jchis@depaul.edu

Joana Diaz
DePaul University, jdiaz113@depaul.edu

Brianna E. Ortiz
DePaul University, bortiz12@depaul.edu

Imani G. Robertson
DePaul University, irobert7@depaul.edu

Jelani A. Shadd
DePaul University, jshadd1@depaul.edu

Stratospheric Effects on UV, Speed of Sound, Pressure, and Temperature

Acknowledgements

The authors of this paper would like to acknowledge the Rising STEM Scholars Program (RSSP) for the resources and facilities provided in conducting our research. We also thank both the Illinois Space Grant Consortium (ISGC) and the DePaul Academic Growth and Innovation Fund (AGIF) for the financial support provided in conducting our research. For the support and guidance in completing this project, we thank our faculty advisor, Dr. Beck-Winchatz.

Stratospheric Effects on UV, Speed of Sound, Pressure, and Temperature

Joshua Chis, Joana Diaz, Brianna Ortiz, Imani Robertson, Jelani Shadd*[1,2]

Department of Physics

Department of Chemistry and Biochemistry

Department of Environmental Science and Studies

Department of Health Sciences

Department of Biology

Dr. Bernhard Beck-Winchatz, PhD; Faculty Advisor

ABSTRACT The atmosphere is composed of several layers, each with its own distinct environment varying in temperature, pressure, and levels of UV radiation. Quantifying these varying parameters proves to be useful in understanding atmospheric composition in greater detail. Variance in the composition of the atmosphere allows for the study of the evolution of physical phenomena at different altitudes. Our group quantified this variance using a high-altitude weather balloon and designed an experimental method to observe the nature of sound propagation through varying altitudes. The goal was to develop an altitude-dependent model of the speed of sound by using an open-air, microcontroller-based payload. Using our platform, we found that the open-air payload design results in noisy readings. Additionally, our method was restricted to low altitude environments, unable to produce reliable data above 6,700 meters. We address possible improvements and constraints in developing an open-air payload design to derive an altitude-dependent model for sound propagation. Furthermore, we present our findings on the variations in pressure, temperature, and levels of UV radiation during balloon flights at altitudes of up to 30,000 meters. These variations included a proportional decrease in pressure, a temperature inversion at 15,000 meters, and an exceptional increase in both UVA and UVB radiation as altitude increases.

[1] Research was completed Summer 2021

[2] Authors listed in alphabetical order

INTRODUCTION

The Earth's atmosphere consists of five major layers. From lowest to highest the layers of the atmosphere are the troposphere, stratosphere, mesosphere, thermosphere, and exosphere. For the purpose of our research, our focus is primarily on the troposphere and the stratosphere. By launching a weather balloon with attached payloads, we look to study the variations in pressure, UV radiation, temperature, and speed of sound at varying altitudes.

The troposphere extends from the Earth's surface to approximately 12 kilometers (7.5 miles) high and contains 99% of all water vapor and aerosols as well as all the air needed for the photosynthesis of plants and aerobic respiration of animals (Buis, 2019). Most of the weather that occurs on Earth happens within the troposphere and all clouds, excluding cumulonimbus thunder clouds, are formed in the troposphere. Almost all of Earth's atmospheric mass is found within the troposphere as it is the densest atmospheric layer due to the compression of weight from the air in the neighboring atmospheric layers. The troposphere has warm air at the bottom and colder air at higher altitudes, which is why the stratosphere is considered to have an inverted temperature profile. The tropopause is located nearly 10,000 meters into the atmosphere and is the location of the temperature inversion present in the atmosphere (Russel, 2011). Here, atmospheric temperature deviates from the declining trend relative to altitude and increases before continuing to decrease once again.

Above the troposphere is the stratosphere, which includes the ozone layer, made of ozone (O_3). Ozone, as a gas, was first discovered by Christian Friedrich Schönbein (1840). In 1913, atmospheric research presented evidence in favor of the idea that there existed a layer of ozone within the atmosphere (Fabry & Buisson, 1913). As scientists continued to research the ozone layer, they were led to evidence of its depletion in the 1970's, and that the main cause was the presence of chlorofluorocarbons (CFC) in the atmosphere (Molina et.al., 1974). Such cases of depletion are found at the greatest extreme above Earth's poles (NASA, 2009). CFCs are human-made gasses which were used for several different purposes such as: refrigerants, solvents, and aerosol sprays. CFCs are organic chemicals which contain carbon, chlorine, and fluorine. Because of this discovery, a push for a decrease in the production of CFCs was started. Doing so would give the ozone layer an opportunity to regenerate, uninhibited by the presence of CFCs. One of the main reasons ozone regeneration is considered a success is due to the unanimous agreement in the United Nations of its merit, leading to the signature of 197 countries (including observing, and non-member countries) onto the Montreal Protocol. Today, this stands as an example for how international policy can positively affect the state of the environment. The Kigali Amendment, signed in 2016, was added to the protocol to reduce the production of hydrochlorofluorocarbons (HCFC), an alternative to CFCs (United Nations, 2016). Without the ozone layer humanity would be exposed to incredible amounts of radiation, for it is the ozone layer which absorbs the majority of harmful ultraviolet (UV) radiation in our atmosphere. UV radiation is a type of radiation emitted from the sun. The ozone layer converts this radiation into heat energy and allows for life in the troposphere.

There are three types of UV radiation, UVA, UVB, and UVC. As shown in Figure 1**,** UVC is completely absorbed by the ozone layer, while a majority of UVB is absorbed, and UVA is left unabsorbed by the ozone layer (WHO, 2016). UVC rays have the shortest wavelengths (100-280nm) which is why they are completely absorbed, while UVA have the longest wavelength (315-400nm), and UVB between them (280-315nm) (WHO, 2016).

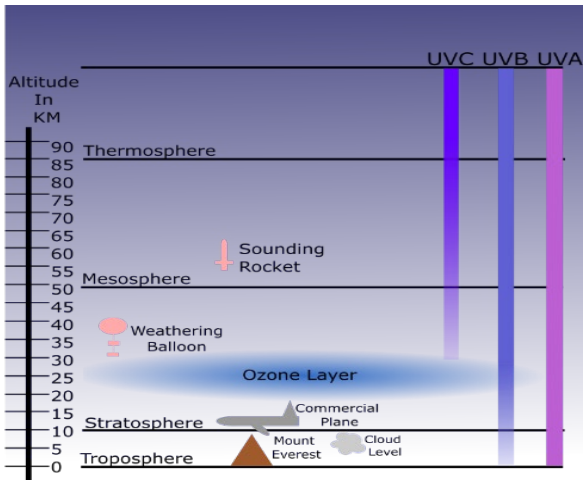

Figure 1 Diagram of the layers of the atmosphere. The ozone layer, residing around 25 km in the atmosphere, successfully filters out UVC rays before reaching the troposphere. However, it is unsuccessful in the complete filtering of UVA and UVB rays.

As altitude increases, atmospheric pressure decreases. There are two reasons for this, the first being that gravity pulls air towards the surface of the Earth, therefore as you get farther from the Earth you will encounter less air and thus less pressure. Secondly, the number of gas molecules decreases as altitude increases. As altitude increases, there is evidently less weight that each layer of the atmosphere has above it which decreases the amount of pressure at that altitude. Equation (1) shows a theoretical model for pressure dependent on height (altitude):

$$P_h = P_0 e \frac{-mgh}{kT} \quad (1)$$

where m is the molecular mass (of air), h is the height (in meters), k is the Boltzmann constant, g is the acceleration due to gravity, T is the surrounding temperature (in Kelvin), and P_0 is the pressure at sea level.

Modern weather balloons are typically made of latex and filled with hydrogen or helium. Due to lower air pressure at higher altitudes, the balloons expand, and eventually burst, finally being brought back down by a parachute. UV radiation, pressure profiles, and temperature profiles can all be recorded by using experimental tools such as weather balloons in combination with sensors. Conducting a balloon launch requires that teams monitor predicted flight paths, weather conditions, and equipment prior to a launch to ensure a proper flight. Websites can be found online, such as Habhub,[3] which allow for flight path predictions to be made given parameters such as launch time, launch site, and predicted ascent/descent rate. Making predictions allows for easier tracking when chasing the balloon for retrieval. Since weather conditions play another key role in conducting high altitude balloon flights having predictions can make retrieval a far more guided activity. Days with violent winds and/or showers make for difficult preparation of the balloon prior to the launch. Additionally, extreme weather in the troposphere and the jet streams found between the troposphere and stratosphere may also derail a balloon's current flight off its predicted path.

Checking flight equipment is another necessary step to ensure a proper flight. These checks include that all data loggers are on and collecting data; especially those responsible for receiving and sending GPS data of the balloon. Properly weighing the payloads of an experiment gauges how much helium it is necessary to put into the weather balloon. Not adding enough helium leads to slow ascents and long flights; thus, it will take longer for the balloon to burst. In the case where the balloon is severely underfilled, the balloon will not ascend at all.

Modern weather ballooning techniques allow for the integration of microcontroller-based systems onto the payloads of high-altitude ballooning experiments. Microcontrollers are compact computing platforms that control the operations of a larger system, application, or circuit and can communicate with an array of sensors to gather data (EIT, n.d.). To communicate the functions of a microcontroller, users must program its functions using an integrated development environment and a programming language compatible with the microcontroller. Companies like Arduino[4] offer platforms that make access to

[3] https://predict.habhub.org/

[4] www.arduino.cc

microcontrollers easy and simple for experimental uses, and mainly use the C++ programming language to program the microcontroller (varies across board models). Microcontroller peripherals such as distance sensors use sound propagation to measure distance. The HC-SR04 ultrasonic distance sensor[5] utilizes ultrasound (40kHz frequency) to measure the distance between the sensor and an object in front of it. It does so by sending an outgoing pulse of ultrasonic sound waves toward a reflective boundary and calculating the distance using the timing between the outgoing pulse and incoming-reflected pulse of the response signal provided by a microphone on the sensor. The microcontroller and ultrasonic sensor communicate by having the microcontroller control the state of the sensor. A sensor in a HIGH state refers to one which is currently sampling data, while a sensor in a LOW state is not currently sampling data.

Sound travels through mediums in the form of pressure waves and is dependent on properties of the medium such as its density and bulk modulus. The speed of a sound wave relates the two prior components as a quotient:

$$v = \sqrt{\frac{\beta}{\rho}} \qquad (2)$$

where β is the bulk modulus of the medium (a measure of its compressibility) and ρ is its density. However, the equation in this form does not work in the context of collecting real time data based on the surrounding environment of a weather balloon. The equation can instead be written in terms of the temperature of the medium by modeling the pressure waves in sound propagation as separate adiabatic processes. This model is appropriate for testing in open air since the pressure waves traverse the media at a rapid enough speed insofar that the system sees no heat exchange within itself. These adiabatic processes are expressed in terms of a product between the pressure and volume of the system in the following form:

$$PV^{\gamma} = \text{constant} \qquad (3)$$

where the superscript γ here is equal to 1.4 and is defined as a ratio of the specific heats of the diatomic molecules found in air. Using this relationship, we can define the bulk modulus as a product of γ and the pressure (P) of the system. Finally, in using the ideal gas law we can substitute the pressure term and write the speed equation in terms of the temperature of the system:

$$v = 20.04\sqrt{T} \qquad (4)$$

In this form, temperature sensors can be leveraged to create speed of sound profiles since the temperature of the surrounding environment of a weather balloon is readily available.

METHODS

For this study, there were a total of three balloon launches separated by a week's time. Our first launch was conducted on July 1st, 2021, the second on July 8th, 2021, and the third on July 14th, 2021. Prior to the flight of the weather balloon an array of payload components including: HOBOware sensors (HOBOware software), which measure temperature, Vernier sensors,[6] which measure UV radiation and gas pressure, GoPro cameras, and an MKRZero Arduino microcontroller[7] programmed to collect sound data, were secured inside of individual payloads (example payload shown in Figure 2). Each of the payloads were attached using six-foot-long strings connected by clips and loops. The payloads were constructed of polystyrene and their lids were tightly secured using a combination of duct tape and zip ties. The strings were run through carbon tubes in each payload. The order in which the payloads were linked, and how the strings connected the payloads, can be seen in Figure 3.

[5] www.sparkfun.com/products/15569
[6] www.vernier.com
[7] https://docs.arduino.cc/hardware/mkr-zero

Figure 2 Example of payload used in launch. This payload has a harness on it to keep it closed during the flight. Atop the payload two UV radiation sensors are placed to collect UV radiation data throughout the flight.

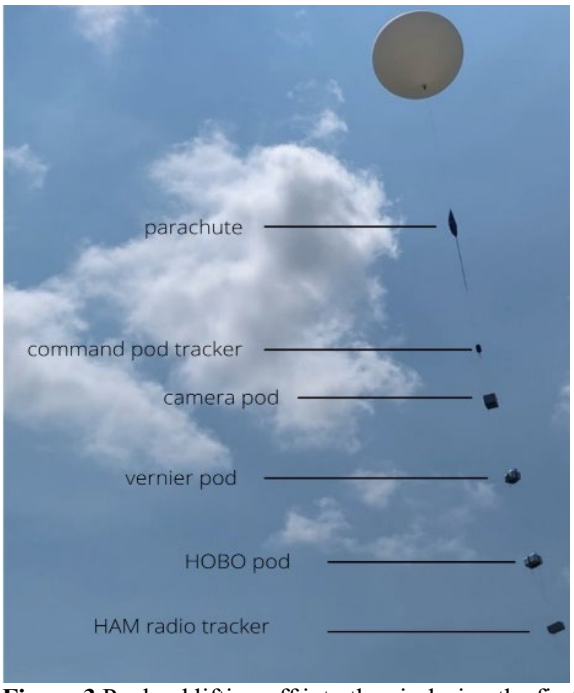

Figure 3 Payload lifting off into the air during the first launch. Each label in the figure refers to a specific payload component used during the launch. During our following flights, the number of payloads differed since we added and/or discontinued the use of specific payloads.

Launch one contained HOBOware temperature sensors, UVA and UVB Vernier sensors, and an air pressure sensor. Launch two contained the HOBOware temperature sensors, three GoPro cameras and the Arduino sound sensor. Launch three included the same payloads as in launch two in order to collect additional profiles on temperature and the speed of sound. All three launches were conducted in a field at Pontiac Township High School in Pontiac, Illinois. Pontiac was chosen since its topography is flat and open, allowing for a secure release and retrieval of the balloon, uninhibited by any towering structures. Prior to each flight, the flight path of the balloon was predicted using Habhub. Predictions depended on latitude, longitude, and altitude of the launch site as well as the time and date of each launch. In addition, the estimated ascent and descent rates as well as the estimated burst altitude are taken into consideration when generating a flight prediction. Figure 3 shows the interface for adjusting flight prediction parameters on Habhub. Habhub predictions account for current weather conditions from a chosen area on a set day and time to determine how the balloon will be carried by the wind. Weather data is made available by the NOAA Global Forecast System (GFS) which uses a mathematical model run four times daily. A final prediction was made the morning of the launch to maximize the accuracy of the predictions. An example prediction is provided in Figure 5.

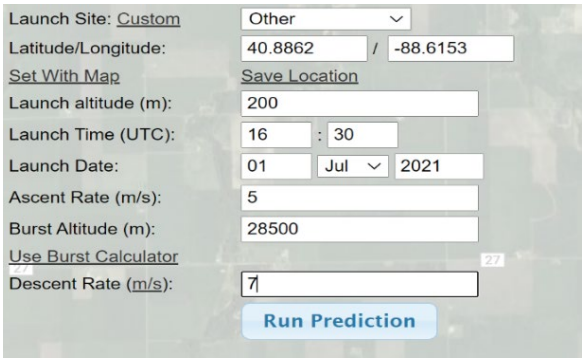

Figure 4 Habhub flight prediction software user interface. Each field corresponds to the specified parameters for a flight. Altering a parameter influences the final predicted flight.

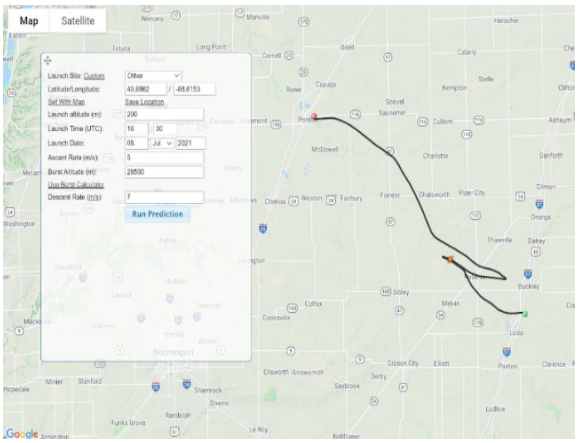

Figure 5 Map of flight prediction for launch two. The sudden change in direction is often due to the winds encountered by the balloon as it ascends through the atmosphere.

During launches where camera payloads were used, each camera was set to record in 1080p resolution and secured into a payload using zip ties. One camera was facing up towards the balloon, one was facing out of the side of the payload, and the last was facing the bottom of the payload, looking back onto the Earth. Views from the side GoPro can be seen in Figure 6, while Figure 7 provides a view from the top GoPro.

Figure 6 Photo taken from one of the balloons on-board cameras showing the earth at nearly thirty-thousand meters

Figure 7 Photo of the balloon bursting; taken by the top-facing camera with the sun in the background. Note how even though the sun is high in the sky, the sky at this altitude is completely dark.

The payload which included the HOBOware temperature sensors collected data throughout the entire launch. Prior to the launch the sensor was programmed to a push button start, with a 5 second sampling interval, recording in units of degrees Celsius. Four temperature sensors were placed in a single payload. One sensor was strapped through the top, one on the right side of the payload, one on the bottom of the payload, and one kept inside of the payload. This was done to create as fine a temperature profile as possible. After the launch was complete, the HOBOware temperature sensors were connected to a computer and then manually stopped using the HOBOware software.

The Vernier data logger was connected to the UVA, UVB, and gas pressure sensors. To set up the data sensors a fully charged Vernier data logger along with analog sensors were connected via a microUSB cable. The data loggers were set to a 2.75-hour window of data capture, capturing 720 samples per hour. This configuration was chosen to have a five second sampling rate throughout the entire flight. At the start of launch preparation, the Vernier data logger was set to begin data collection before closing the payload. Predictions for gas pressure, UVA, and UVB concentrations were made prior to launch, and comparisons were made post-launch.

Our goal for the experimental payload was to design an experiment in which the testing

environment best matched the surrounding atmospheric conditions. Thus, an open-air payload design was implemented, allowing for direct access to the surrounding atmospheric environment. Figure 8 (a) and (b) show the payload design. (a) and (b) show that windows were cut on opposite sides to allow continuous air flow through the testing environment. The two remaining sides of the payload were used for testing our sound experiment. On one side (left of (a)) a breadboard holding our microcontroller and ultrasonic distance sensor was hot glued onto the bottom pane of the payload. To collect speed of sound measurements we utilized the HC-SR04 ultrasonic distance sensor. We fastened the wires connecting the microcontroller and sensor by an additional application of hot glue. Opposite to the sensor (right of (a)), a rigid plastic board was secured onto the remaining wall of the payload (again, by using hot glue), acting as the reflective boundary for the sensors outgoing sound impulses. This reflective boundary would allow the sound impulses sent out from the sensor to travel through the air and back to the sensor. Similar methods for observing the effects of altitude on the speed of sound have been taken on before as seen in the work done by Adam Chase et al. in 2017. Having these two windows cut out of the payload was necessary to ensure a robust model of the variation in the speed of sound at higher altitudes and lower temperatures since the testing environment (payload interior) mirrored the current conditions in the atmosphere.

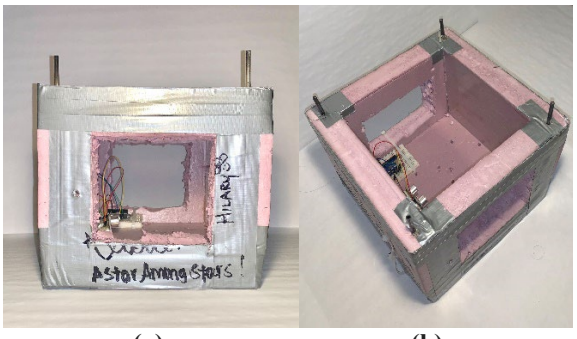

(a) **(b)**

Figure 8 The open-air payload design. **(a)** shows a side view of the payload. **(b)** shows an angled view of the experimental payload. A plastic reflective boundary was used due to its immediate availability and tendency to not completely absorb the sound impulse.

We used the Arduino MKRZero microcontroller and HC-SR04 ultrasonic distance sensor to measure and collect data on the speed of sound. The MKRZero can operate in a power efficient mode while running and can store data onto an embedded SD card. We powered the board using a mobile power bank which provided five volts to the board throughout the entire flight. To enable the functionalities of our microcontroller and sensor we wrote a program in C++ which calculated the speed of sound given the data generated by the distance sensor and appended the speed measurements line by line onto a text file saved onto the embedded SD card. The program was designed in accordance with the specifications of the HC-SR04 sensor and enabled the trigger pin for a 10-microsecond period, which sent out a sound impulse, disabled the trigger pin, and finally set the echo pin status to HIGH, allowing the sensor to obtain the signal from the microphone on the sensor once the sound impulse rebounded off the reflective boundary. These sensors, however, are traditionally used to measure distance, and in doing so presupposes a speed of sound (343 m/s). By keeping the distance between the sensor and reflective boundary invariant we alter the sensors' functionality to primarily time the sound impulse, acting as a high-altitude stopwatch. With distance being constant and the sensor providing the time of travel, the speed can trivially be calculated by dividing the distance traveled by time of flight of the sound impulse. We implemented this program architecture within an infinitely running loop to generate a complete dataset throughout the flight. The only time that execution of the code would stop is once the mobile power bank was disconnected from the microcontroller. Altogether, the sensor would send out an impulse of sound, record the time it took to travel to the reflective boundary and bounce back to the microphone, and compute the speed given the invariant distance and the sensed time. Error checks were also implemented into the program. In the event of an encountered error within the program, an LED indicator would begin to blink. Prior to each flight the indicator would be checked. If the indicator did not turn on, that meant the program was successful in beginning to write data onto the onboard SD card.

One of the trackers used was a HAM Radio Tracker.[8] This tracker was hanging at the bottom of the chain of payloads so the antenna from the tracker could communicate with amateur radio stations. GPS coordinates of the balloon were uploaded to aprs.fi.[9] We used the balloon's radio callsign and aprs.fi as one of our methods to tracking the balloon's flight. The second tracker we used was a 900 MHz Stratostar Command Pod.[10] This tracker was placed directly under the parachute and was the main device used for tracking the balloon. It operates by transmitting information packets to the chase vehicle's antenna. Packet information sent from the tracker includes current GPS co-ordinates, temperature and pressure values, and updated ascent/descent rate values. A receiver antenna was placed atop the chase vehicle and connected to a laptop where we received the balloon's updated information packets in six-second time intervals. This tracker also logged the altitude throughout the entire flight. Both the HAM Radio Tracker and the Stratostar Command Pod provided real-time data which allowed us to monitor the ascent and descent rate of the balloon through its flight.

Upon arrival to the launch site, the team coordinated the setup of the balloon, hooking up the helium tank, prepping payloads, and turning on all sensors. Once all sensors were running, the payloads were hooked together using clips tied to the lines joining all the payloads together. The balloon was then filled with the helium while one person held onto the neck of the balloon. Holding onto the neck is a measure taken to ensure minimize the leakage of helium out of the balloon and to make sure the balloon does not fly off while being inflated. A photo of the filling process is shown in Figure 9. We measure the lift of the balloon by using a digital fish scale hooked to the neck of the balloon. After measuring a lift appropriate for our desired ascent rate, we close off the neck of the balloon using multiple zip ties to ensure that no helium leaks out during the flight. Once everything is set, the balloon is walked out to an area free of any towering structures that could potentially intercept the balloon during its ascent. Slowly, each of the lines are let go, letting one payload reach the air at a time to ensure that none of the lines are tangled. Once the entire balloon and many of the payloads are in the air, the balloon is let go. The balloon is then tracked via the onboard GPS.

Figure 9 The research team preparing a flight by filling up the balloon. As seen in the figure, one person must hold the balloon at the base during the filling period to stabilize the balloon. Note gloves are worn during the filling process as to not place any oil onto the latex of the balloon.

After the balloon is launched, we set out in a chase vehicle and follow the general path of the balloon using the GPS data provided by one of the two onboard trackers. Figure 10 shows a 3D model of the balloon's flight path, made using the GPS data provided. Using the prediction as a reference, and observing how the balloon moves during its flight, we determine a general landing area to drive towards for retrieval upon the balloon's descent to the ground. Once it is noted that the ascent rate begins to decrease and approach zero, we know that the balloon is beginning its descent. This indicates that the balloon has burst and is now enroute back to the ground using the attached parachute. As the balloon approaches the ground, the HAM radio tracker becomes useless since the balloon is eventually lower than the radio towers and is unable to send a signal. Once the balloon reaches the ground, we use the last sent GPS coordinates

[8] https://shop.bigredbee.com/products/2-meter-5-watt-aprs-transmitter

[9] https://aprs.fi/

[10] https://stratostar.com/meet-stratostar/

provided by the Stratostar command pod to find the popped balloon and payloads. The usual trip distance from the launch site to the landing site was close to 50 miles taking local routes. Typically, the balloon would land in open fields, with a one-time exception in our experience of it landing in a cornfield.

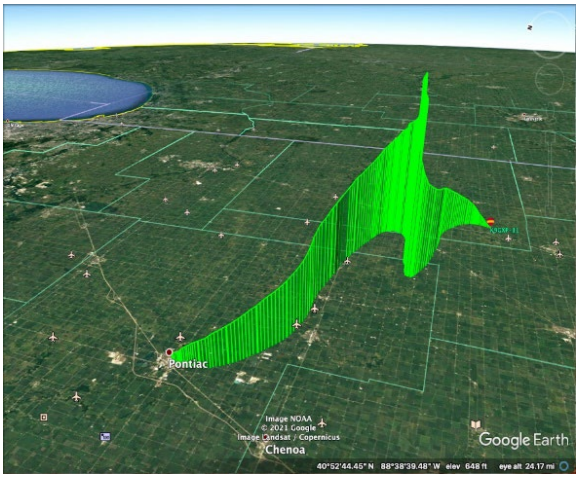

Figure 10 A 3D model of one of the flight paths. Note the curvature of the path after reaching the maximum altitude. This is due to the change in wind directions encountered by the balloon at different altitudes.

Once located and retrieved, the balloon is taken back to the chase vehicle where the payloads are disassembled, and data storing components (SD cards for GoPro cameras and Microcontrollers) are retrieved for later analysis. Figure 11 displays the balloon and payloads after retrieval along with the authors.

Figure 11 The research team after recovering the balloon from the second launch. This flight landed onto a local farmer's property, where we were met welcomingly by their dogs and family.

RESULTS

Our research group conducted three balloon launches over the span of three weeks. The three launches varied such that on our third and second launch we deployed our experimental payload. On our first launch, on July 1st, 2021, we collected data on temperature, pressure, and UV radiation. During our second launch on July 8th, 2021, we collected data on temperature and the speed of sound. Additionally, a camera payload was added. The last flight on July 14th, 2021, collected data on temperature, the speed of sound, imaging data, humidity percentage, and pressure. Note however that humidity and pressure data were taken by an extension board for the on-board microcontroller. This data was only used in an effort to understand possible errors in the speed data. In addition, all flights captured altitude data from the flight; logged by the onboard StratoStar Command Pod. An interpolation was done during post flight analysis to fit sensor data to the accompanying altitude data. This was necessary since the sampling rates between the two data sets differed. Figures 12, 16, and 18 show the temperature data recorded from launches one, two, and three respectively. In each figure we identify where the sensor was placed within the payload. Placement of the sensors were varied to generate as accurate a temperature profile as possible. Figures 17 and 19 show the speed of sound data collected on launch two and three, respectively. Figure 15 shows the pressure data collected from launch one, and Figures 13 and 14 show the UV radiation data from launch one.

As a result of our post-flight analysis, sensor failures were found in two of our three launches. In our first launch, a temperature sensor which captured the temperature profile of the side of the payload failed. As a result, Figure 12 has one less data series than Figures 16 and 18. In launch three, the balloon missed its altitude target which resulted in a smaller set of temperature data present in Figure 18. The ultrasonic sensor installed in our experimental payload failed early on in our first launch; only reliably generating data for the speed of sound below 2300 meters. Either due to saturation or obstruction of the sensor, our UVB radiation data from the first

launch was inaccurate past 9000 meters, thus Figure 13 omits any of this data; only showing UVB radiation data up to 9000 meters.

Launch One (07/01/2021)

Results from the analysis of the temperature data from launch one agreed with the background the team had on the atmosphere's composition. We expected that within the tropopause (~ 15 km) a temperature inversion should take place. Figure 13 shows that the temperature of the surrounding environment begins to stagnate at 15 kilometers then finally inverts at 19.2 kilometers. Table 1 summarizes the range of temperature values recorded between all temperature sensors in launch one.

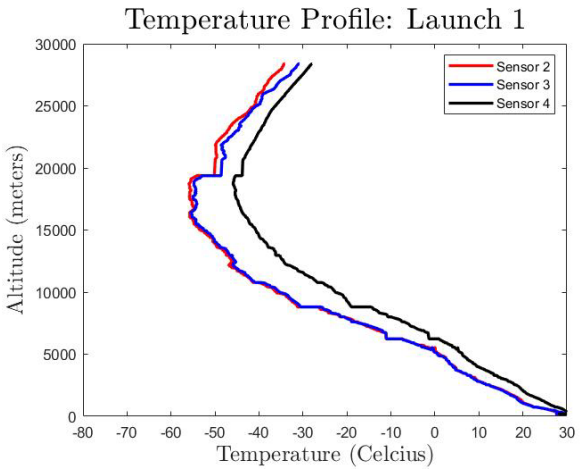

Figure 12 Temperature profile collected from launch one. Sensor 2 (red) was sticking out of the bottom of the payload. Sensor 3 (blue) was sticking out the top of the payload. Sensor 4 (black) was placed inside of the payload. Note that sensor 1 had failed during launch one.

	Minimum Temperature	Maximum Temperature
C°	-58	35
F°	-72.4	95

Table 1 Highest and lowest temperatures captured from all sensors in the payload for Launch one. The range of the values is 93° (Celsius).

The first launch included a payload that held the UV sensors connected to the Vernier LabQuest2 datalogger. UV radiation data obtained from the launch agreed with our prediction of seeing comparably lower levels of UVB than UVA during the entire flight due to the absorption of UVB by the ozone layer. Additionally, we expected to find that levels of both UVA and UVB would increase with altitude and decrease relatively at lower altitudes. Table 2 addresses this relative decrease in relation to altitude and UVB radiation. Consistently, the UVB readings decrease with altitude and decrease relatively at larger and larger percentages as altitude decreases. There were many discrepancies in the data for UVB radiation, however. We found that many data points were not consistent or accurate. The reasons for this is that the sensor may not have been equipped to collect data past a certain range in milliwatts per square centimeter, or the payload that carried the sensors may have been blocked by another payload above it, causing an obstruction to the sensor, and thus inaccurate data points to be collected. During data analysis, the inaccurate data points were ignored to create graphs of the relationship between altitude and UVA/UVB, which is shown in Figures 13 and 14.

Altitude (m)	UVB $\left(\frac{mW}{cm^2}\right)$	Percent Difference (±%)
8806	995.845	N/A
7120	946.289	− 4.976
4997	806.089	− 14.816
2988	684.316	− 15.107
1005	467.168	− 31.732

Table 2 Percent difference in UVB Radiation. We see as we descend in altitude the magnitude of the percent difference increase by two times and greater. Note that readings have been rounded to the nearest thousandth, and altitudes to the nearest whole number.

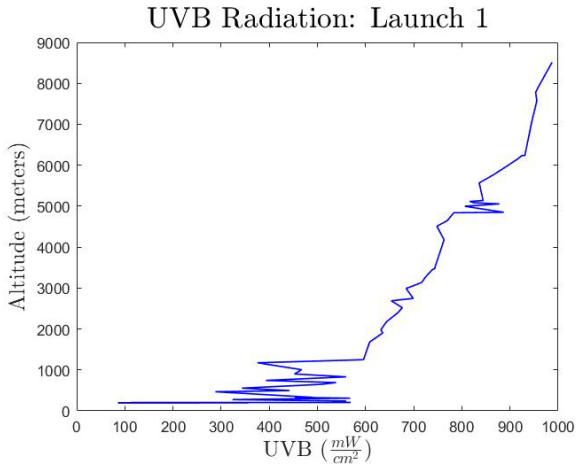

Figure 13 UVB radiation data collected from the on-board sensor. Data from the balloon's descent has been omitted. The UVB sensor used in this payload began to saturate at the 9000m altitude target. As a result, the data collected above this target is omitted.

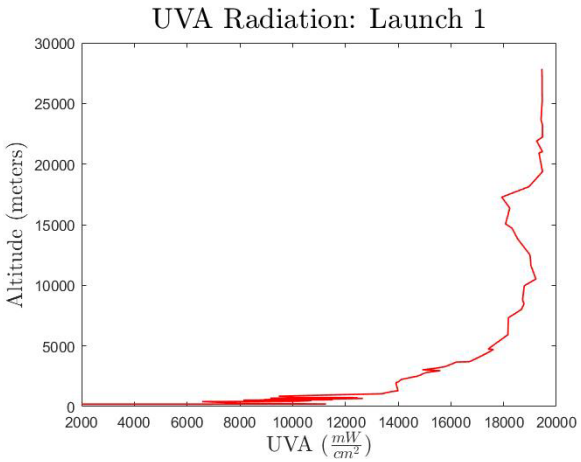

Figure 14 UVA radiation intensity data collected from the on-board sensor. Data from the balloon's descent has been omitted. Trends show radiation levels rise in tandem with altitude, in line with expectations.

The data collected on UVA radiation levels show a dramatic increase in the levels of UVA radiation past the 5000-meter altitude mark. At this altitude, the balloon is still in the troposphere, not yet passing through the ozone layer. Once the balloon reaches the stratosphere ($\approx$ 10,000 meters) an apparent deviation from the general trend, and increase, in UVA is observed. This can be due to the balloon's passing through ozone, thus filtering (minimally) the UVA meeting the sensor. Table 2 summarizes the trend in UVA radiation by showing the percent difference in radiation levels as altitude decreases. The differences between the maximum readings between UVA and UVB show the tendency of the Ozone layer to mainly filter UVB radiation. The maximum reading in UVB radiation was 1005.806 mW/cm^2 while the maximum reading in UVA radiation was 19445.093 mW/cm^2.

Altitude (m)	UVA $\left(\frac{mW}{cm^2}\right)$	Percent Difference (±%)
25225	19464.331	N/A
23226	19473.950	+ 0.049
20914	19339.282	− 0.692
19376	19473.950	+ 0.696
17271	17930.078	− 7.928
15065	18074.365	+ 0.805
12553	18983.374	+ 5.029
10517	19223.853	+ 1.267
8007	18675.562	− 2.852
5921	18160.938	− 2.756
4210	17194.214	− 9.667
2033	14005.469	− 18.545
496	10710.913	− 23.523

Table 3 Percent difference in UVA radiation. We see as we descend in altitude the percent difference is not uniformly negative. From 15000 down to 10500 meters, we find a period of increase in the UVA radiation levels. In this altitude range atmospheric filtering was increased leading to a drop in radiation levels. Note that readings have been rounded to the nearest thousandth, and altitudes to the nearest whole number.

The pressure data collected was consistent with equation (1) with a slight deviation forming as altitude increased. We found that as altitude increased, gas pressure decreased. This is in line with what is expected from the composition of the atmosphere. With the density of air being inversely correlated to altitude, we should expect that pressure drops with density. Figure 15 shows the pressure profile from launch one. Table 4 summarizes how pressure deviated from the theoretical prediction from the three major points of the balloon's flight: launch site, midpoint of flight, and maximum altitude of fight.

Altitude (m)	Experimental Value (kPa)	Theoretical Prediction (kPa)
0	98.87	98.520
16000	10.29	8.14
28298	3.00	1.93

Table 4 Summary of the deviation in experimentally observed values of pressure from theoretical predictions for launch one. The sensor evidentially diverged farther from the theoretical prediction as altitude increased. Note altitude here is relative.

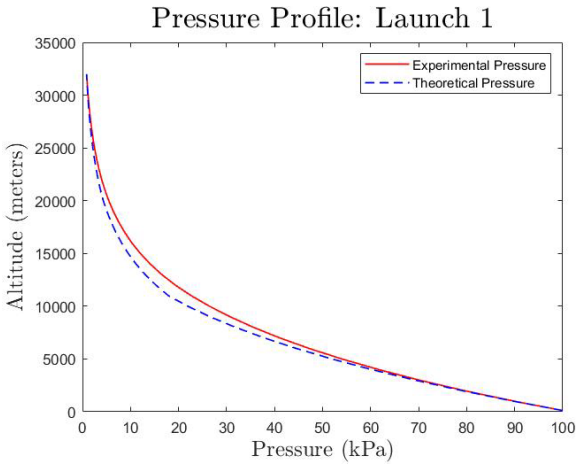

Figure 15 Pressure data collected from the on-board sensor. We find a higher divergence from theoretically expected values in the altitude range of 10 to 20 kilometers. Note altitude here is relative to the initial altitude of the sensor.

Launch Two (07/08/2021)

In the analysis of launch two's temperature data, a finer temperature profile was found since all four sensors in the payload were operational. Different from launch one's temperature inversion, the inversion found in launch two was far more abrupt, void of any period of stagnating temperature. The inversion took place at 15.7 kilometers; 4.5 kilometers earlier than in launch one. Figure 16 shows the full temperature profile of launch two. Table 5 summarizes the range of temperature values recorded between all temperature sensors in launch two.

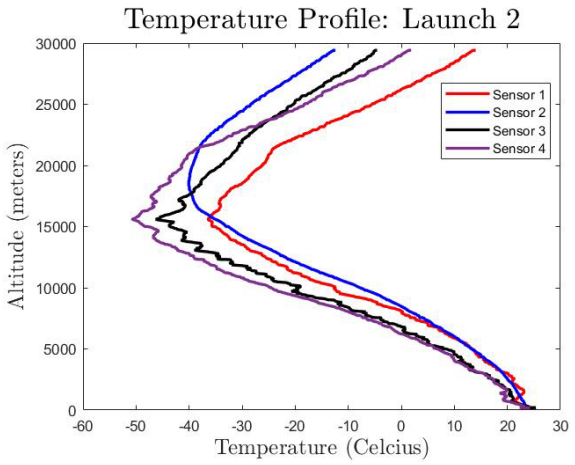

Figure 16 Temperature data collected from launch two. Sensor 1 (red) was sticking out of the bottom of the payload. Sensor 2 (blue) was placed inside of the payload. Sensor 3 (black) was sticking out of the side of the payload. Sensor 4 (purple) was sticking out of the top of the payload.

	Minimum Temperature	Maximum Temperature
C°	-57.33	27.33
F°	-71.50	81.14

Table 5 Highest and lowest temperatures captured from all sensors in the payload in launch two. The range of the values is 84.66° (Celsius).

The data provided by our ultrasonic distance sensor showed that our sensor failed early in the flight. In launch two, the data provided by the microcontroller consistently diverged from our theoretical model (equation (4)) after 2300 meters. Figure 17 shows a plot of the data provided by the microcontroller as well as the relative error from our theoretical model.

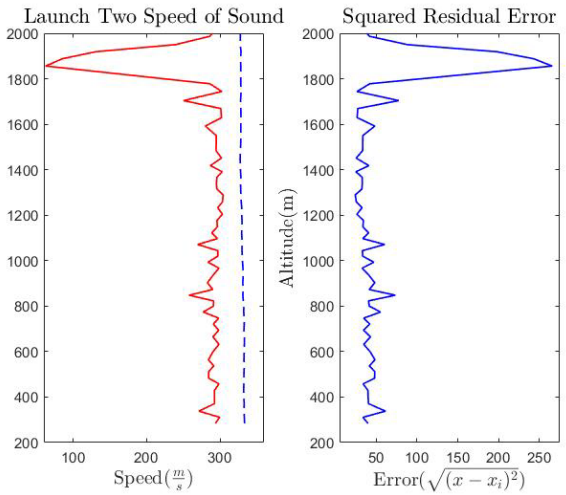

Figure 17 Speed of sound data collected by the on-board microcontroller from launch two. The left-most graph displays the experimental speed measurement (red) and the theoretical value (dotted blue) derived from equation (4). The right-most graph displays the error (blue) in the readings relative to the theoretical model. Launch two showed minimally noisy readings in low-altitude environments, however, were off by a near constant (≈ 50). The error present in the readings increase dramatically once the payload reaches altitudes of 1600 meters and higher.

Figure 17 clearly shows that the experiment produces unreliable data at altitudes higher than 1600 meters. To provide a measure of the experiment's reliability, the average of the squared residuals[11] was computed for the altitude range that the sensor was functional (0-2300 meters). This average for launch two was 23.24. After launch two we altered the code uploaded to the microcontroller to better account for the change in environmental conditions that the experiment would endure during flight.

Launch Three (07/14/2021)

Launch three did not reach as high of an altitude as the other launches (maximum altitude was 24 kilometers) which is why its altitude data stops before 30 kilometers. The temperature sensors left the troposphere at about 15 kilometers, which can be seen by the temperature inversion on Figure 18.

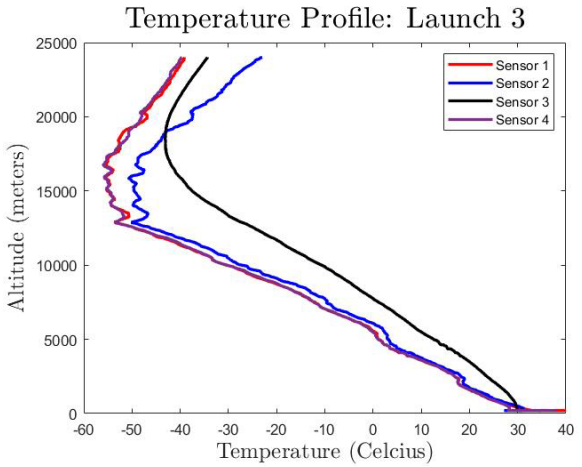

Figure 18 Temperature data collected from launch three. Sensor 1 (red) was sticking out of the side of the payload. Sensor 2 (blue) was sticking out of the top of the payload. Sensor 3 (black) was placed on the inside of the payload. Sensor 4 (purple) was sticking out of the bottom of the payload.

It can be seen from Figure 18 that the sensor which was placed on the inside of the payload generates a much finer temperature profile compared to those generated by sensors placed on the outside. This is true for all three launches. Table 6 summarizes the range of temperature values recorded between all temperature sensors in Launch three.

	Minimum Temperature	Maximum Temperature
C°	-58.32	37.92
F°	-72.98	100.26

Table 6 Highest and lowest temperatures captured from all sensors in the payload for Launch three. The range of the values is 96.24° (Celsius).

Adjusting for the errors present in the speed of sound data from launch one resulted in an improved data set. On our third launch we saw a reliable data stream up to 6703 meters from the experimental payload. After this altitude, consistent divergence was observed in the data and the sensor had clearly failed. During the descent of launch three the data stream became reliable once again at altitudes of 3820 meters and lower. This return to a sensible data stream was not observed in the case of launch two. We found

[11] Relative to the model provided by equation (4)

that after adjusting our code a general increase was observed in the data's tendency to follow our theoretical model (equation (4)). Comparatively, the speed of sound data set in launch two (up to 6703 meters) had an average square residual of 11.26; giving a 51% increase in accuracy at altitudes lower than 7 kilometers. Figure 19 evidentially shows the increase in accuracy found after adjusting the microcontrollers code.

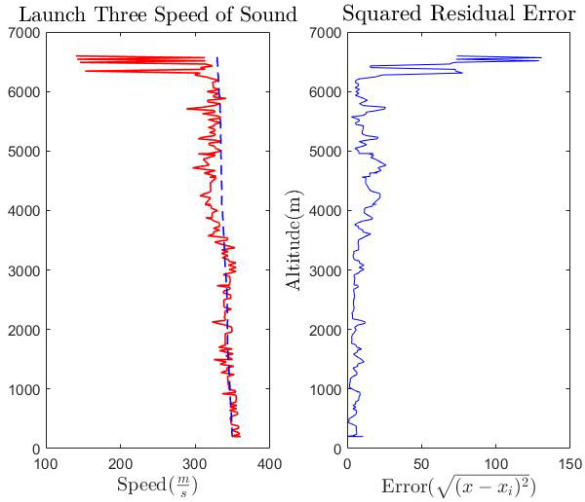

Figure 19 Speed of sound data collected by the on-board microcontroller from launch three. The left-most graph displays the experimental speed measurement (red) and the theoretical value (dotted blue). The right-most graph displays the error (blue) in the readings relative to the theoretical model. Launch three showed significant improvement in the efficacy of our payload design in low-altitude environments. Note the error was put through a moving average (k = 3) to improve clarity in the nature of the error relative to altitude.

DISCUSSION AND CONCLUSION

Much of the data from our launches aligned with the background information behind the composition of the atmosphere. All temperature data shows an inversion within the fifteen-to-twenty-thousand-meter range. Pressure readings showed an appropriate leveling off near the theoretically expected values. However, we were not able to accurately produce an altitude-dependent model of the speed of sound above 6703 meters. Thus, there were several unaccounted-for issues that we ran into throughout the course of the experiment.

Temperature and UV sensor failures were among these issues. Collecting UV radiation data proved to be a challenge, giving rise to a question of how we can ensure that the sensors always have unobstructed access to the surrounding environment. In trying to answer this question it must be noted that the nature of high-altitude ballooning can be unpredictable. Payloads will always sway and partially obstruct those below them. Another issue which occurred during these experiments was with the HC-SR04 Ultrasonic Distance Sensor which was unable to accurately measure the time it took the sound to travel during the duration of the balloon's flight above 2300 meters in launch two and 6703 meters in launch three. We are uncertain why this occurred, but some possible causes are the cold temperatures reached at high altitudes, the low density of air particles at high altitudes, and the movement of the payload during flight. Though equation (4) is modeled to take advantage of open access to the surrounding temperature in the atmosphere, the components of the sensor may not be able to operate given the extreme conditions encountered at high altitudes. Datasheets from sensor manufacturers explaining the operation temperature range of the sensor state that the sensor can operate in conditions of negative fifteen degrees Celsius.[12] Even if we are to assume that all manufacturers share a common operational temperature range, the fact remains that the sensor was not operational at altitudes (≈9 kilometers) where these temperatures are encountered. This may lead to the possibility that the cause of the error is in fact due to the low temperature and air pressure. Equation (4) tells us that we should expect the speed of sound to decrease in accordance with the temperature. Thus, the sampling interval would need an adaptive way to reconfigure itself to wait longer for responses from the reflected impulse. Figure 20 situates the period of failure in the data stream in the same window of time where we encounter drops in pressure, and temperatures below zero degrees Celsius. At ground levels we assume that the sound propagates fast enough to reach the

[12] www.piborg.org/sensors-1136/hc-sr04

sensor in time (which it does). However, this assumption may not hold at 9, 10, and 20 kilometers. The improvement between launches was due to a change in how we collected the data on the speed of sound as opposed to letting the microcontroller calculate the speed and give a data point as was done in the first launch. We decided instead to have the time traveled recorded and use that to calculate the speed of sound ourselves during analysis. Further testing of this experiment would require a method of sustaining the sensor's functionality at cold temperatures without interfering with the surrounding testing environment (ruling out any heating elements for the sensor). Other solutions may include using sensors already designed for very low temperatures, which are commonly used in more industrial contexts for manufacturing. Overall, our attempt at using microcontrollers and sensors to quantify physical phenomena at extreme altitudes is a novel and inexpensive way to approach this study of sound.

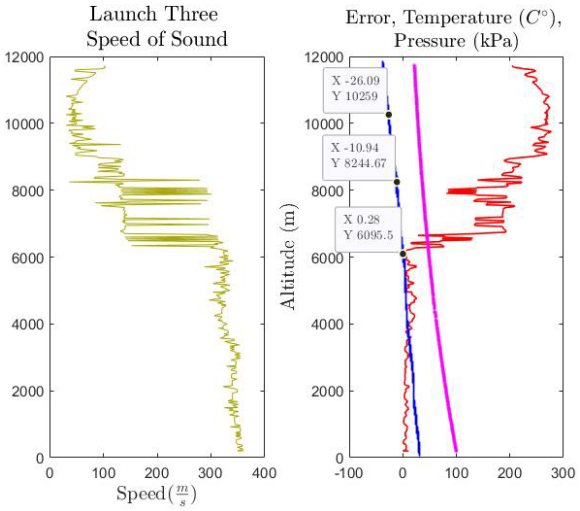

Figure 20 Error analysis of the speed of sound measurements obtained from launch three. The left-most graph displays the computed speeds from the data. The right-most graph displays the error from equation (4) (red), the pressure of the surrounding environment (pink), and the temperature of the surrounding environment (blue). Note that the temperature gradience has been highlighted by the data tips of the right-most graph, showing that relative error increases while temperature drops.

In addition to the temperature sensors and microcontroller, the Go-Pros also experienced some malfunctions due to temperature changes. During the second launch one of the cameras turned off and stopped recording mid launch, only collecting some of the launch footage. Our usage of three cameras minimized the possible loss of footage. Though these issues occurred, the results of our experiment did align with our expectations according to our background research on the atmosphere. Future studies may want to consider taking the time to figure out exactly what range of conditions the devices used in the experiment can operate in to minimize the potential for sensor failure and maximize the amount of data that can be collected.

Further applications of our research include the possibility of in-depth atmospheric composition research. The ballooning platform allows for real time data aggregation of multiple environmental parameters such as temperature, UV radiation, and a multitude of other variables. Using the speed of sound experiment in conjunction with this data may be applicable in seeing the difference between highly polluted pockets of air and clean air for example. Asking the question of what effect, if any, does the density of air pollutants have on the physical process of sound propagation. Since sound propagation primarily relies on the medium through which it travels, considerable information can be taken away from a stable method of analyzing the differences in its travel through different, possibly polluted, media. Similar experiments have been conducted recently in NASA's latest Perseverance mission (Good et.al., 2021). By conducting sound-based experiments researchers found that the reality of Mars' atmosphere differed from their intuition. In summary, using high altitude ballooning as a means of real time data collection is an inexpensive and convenient way of characterizing the atmosphere allowing for a better understanding of its environment.

ACKNOWLEDGEMENTS

The authors of this paper would like to acknowledge the Rising STEM Scholars Program (RSSP) for the resources and facilities provided in conducting our research. We also thank both the Illinois Space Grant Consortium (ISGC) and the DePaul Academic Growth and Innovation Fund (AGIF) for the financial support provided in conducting our research. For the support and guidance in completing this project, we thank our faculty advisor, Dr. Beck-Winchatz.

REFERENCES

Buis, A. (2019, October 16). Earth's atmosphere: A multi-layered cake. NASA. Retrieved February 2, 2022, from https://climate.nasa.gov/news/2919/earths-atmosphere-a-multi-layered-cake/

Chase, A., Dever, W., Foltz, M., Morgan, T., Schaefer, B., Schaefer, B. & Li, Z. (2017). Measurement of speed of sound profile using LaACES balloon. *Academic High-Altitude Conference 2017*.

Fabry, C. & Buisson, H. (1913). Ultraviolet absorption by ozone and the limit of the solar spectrum. *Journal de Physique Théorique et Appliquée*, 3, 196-206. https://doi.org/10.1051/jphystap:019130030019601

Good, A., Fox, K., & Johnson, A. (2021, October 18). Hear sounds from mars captured by NASA's perseverance rover. NASA/JPL-Caltech. Retrieved May 31, 2022, from https://www.nasa.gov/feature/jpl/hear-sounds-from-mars-captured-by-nasa-s-perseverance-rover

Molina, M.J. & Rowland, F.S. (1974). Stratospheric sink for chlorofluoromethanes: Chlorine atom-catalysed destruction of ozone. *Nature*, 249, 810–812.

NASA. (2009, April 10). Ozone: What is it, and why do we care about it? Retrieved May 10, 2022, from www.nasa.gov/audience/foreducators/postsecondary/features/F_Ozone.html

Russell, R. (2011). The Troposphere. UCAR Center for Science Education. Retrieved May 10, 2022, from https://scied.ucar.edu/learning-zone/atmosphere/troposphere

Schönbein, C. F. (1843). On the odour accompanying electricity, and on the probability of its dependence on the presence of a new substance. *Abstracts of the Papers Printed in the Philosophical Transactions of the Royal Society of London*. 4, 226-226. https://doi.org/10.1098/rspl.1837.0114

Types and applications of microcontrollers. (n.d.). Engineering Institute of Technology (EIT). Retrieved May 5, 2022, from https://www.eit.edu.au/resources/types-and-applications-of-microcontrollers/.

United Nations (UN). (2016, October 15). United Nations meeting in Kigali, Rwanda, October 15, 2016. Retrieved May 5, 2022, from https://treaties.un.org/doc/Treaties/2016/10/20161015%2003-23%20PM/Ch_XXVII-2.f-English%20and%20French.pdf

WHO. (2016, March 9). Radiation: Ultraviolet (UV) radiation. Retrieved May 10, 2022, from https://www.who.int/news-room/questions-and-answers/item/radiation-ultraviolet-(uv)